Chemical Science

ROYAL SOCIETY OF CHEMISTRY

EDGE ARTICLE

New pyrido[3,4-b]pyrazine-based sensitizers for efficient and stable dye-sensitized solar cells†

Weijiang Ying,‡[a] Jiabao Yang,‡[ab] Mateusz Wielopolski,[c] Thomas Moehl,[b] Jacques-E. Moser,[c] Pascal Comte,[b] Jianli Hua,*[a] Shaik M. Zakeeruddin,*[b] He Tian[a] and Michael Grätzel*[b]

A series of new pyrido[3,4-b]pyrazine-based organic sensitizers (**PP-I** and **APP-I–IV**) containing different donors and π-spacers have been synthesized and employed in dye-sensitized solar cells (DSSCs). The absorption spectra properties of dyes are analysed by density functional theory (DFT). The calculated results in combination with the experiments suggest that the absorption characteristics and excited state features will mainly be dominated by charge transfer transitions from the highest occupied molecular orbital (HOMO) to the lowest unoccupied molecular orbital (LUMO) and to higher LUMO orbitals. Furthermore, attaching the octyloxy groups significantly extends the π-conjugation of the donor in **APP-IV**, which raises the HOMO energy and facilitates its oxidation. As a consequence, **APP-IV** exhibits the lowest HOMO–LUMO energy gap among all dyes, which, in turn, corresponds well with the red shift of the absorption spectra. Transient photovoltage and photocurrent decay experiments as well as electrochemical impedance spectroscopy indicate that the electron lifetime and charge recombination resistance are increased due to the introduction of octyloxy chains on the donor unit, resulting in the high photovoltage based on **APP-IV**. It was found that **APP-IV** based DSSCs with liquid electrolyte display the highest power conversion efficiency (PCE) of 7.12%. Importantly, a PCE of 6.20% has been achieved for **APP-IV** based DSSCs with ionic-liquid electrolytes and retained 97% of the initial value after continuous light soaking for 1000 h at 60 °C. This renders these pyrido[3,4-b]pyrazine-based sensitizers quite promising candidates for highly efficient and stable DSSCs.

Introduction

After Grätzel and co-workers' first reports in 1991,[1] for the recent past decades, dye-sensitized solar cells (DSSCs) have attracted significant attention as alternatives to conventional solar cells due to their facile and low-cost fabrication combined with high performance.[2] Among all the components of a DSSC, the sensitizers play the key role in achieving high power conversion efficiencies (PCEs) and have, therefore, been intensively studied. To date, DSSCs based on ruthenium-complexes have shown certified PCE values of 11.9%,[3] whereas zinc–porphyrin co-sensitized DSSCs hold a new PCE record of 12.3%.[4]

[a]Key Laboratory for Advanced Materials and Institute of Fine Chemicals, East China University of Science and Technology, Shanghai 200237, People's Republic of China. E-mail: jlhua@ecust.edu.cn; Fax: +86 21 64252758; Tel: +86 21 64250940

[b]Laboratory for Photonics and Interfaces, Institute of Chemical Sciences and Engineering, Ecole Polytechnique Fédérale de Lausanne, CH-1015 Lausanne, Switzerland. E-mail: shaik.zakeer@epfl.ch; michael.graetzel@epfl.ch

[c]Photochemical Dynamics Group, Institute of Chemical Sciences and Engineering, Ecole Polytechnique Fédérale de Lausanne, CH-1015 Lausanne, Switzerland

† Electronic supplementary information (ESI) available. See DOI: 10.1039/c3sc51844b

‡ These authors contributed equally to this work.

Compared to the metal-complex sensitizers, alternative metal-free organic sensitizers[5] have attracted increasing attention due to their high molar extinction coefficient, tunable absorption properties, relatively high efficiency and low cost. Commonly, such organic sensitizers are synthesized by designing a donor–π–acceptor (D–π–A) configuration,[6] owing to their efficient intramolecular charge transfer (ICT) properties. Furthermore, it is well established that for efficient solar energy conversion it is necessary to utilize dyes that possess high charge carrier mobility, broad absorption spectra and long-term stability. Recently, a series of novel D–A–π–A organic dyes[7] incorporating additional acceptors such as diketopyrrolopyrrole,[8] bithiazole,[9] isoindigo,[10] benzothiadiazole,[11] benzotriazole,[12] and quinoxaline[13] into the traditional D–π–A structure were reported and are receiving increasing attention. Inserting an auxiliary acceptor, which acts as an electron trap and increases the efficiency of charge separation facilitates electron transfer from the donor to the anchor. Other consequences of a second acceptor moiety are often broader spectral ranges and enhanced stabilities. Relatively high efficiencies of nearly 9% have already been reported on DSSCs based on this type of sensitizers.[11a] Such promising results drive the quest to find new and appropriate additional acceptors for such D–A–π–A type dye structures.

Pyrido[3,4-b]pyrazine (PP)[14] exhibits a well-known electron-withdrawing effect due to its two symmetric unsaturated nitrogen atoms and the pyridine N-atoms. It has already been widely utilized and shows promising photovoltaic properties in polymer structures for NIR light-emitting diodes,[15] field-effect transistors,[16] two-photon absorption[17] and bulk heterojunction solar cells.[18] Thus, using PP units as components in organic sensitizers is a very attractive approach in terms of their diverse structural modifications and the intrinsic strong electron-deficient properties. To the best of our knowledge, the potential of the PP moiety as an auxiliary acceptor for DSSCs has not yet been explored.

The most popular methods of structural modification for fine-tuning the highest occupied molecular orbital (HOMO) and the lowest unoccupied molecular orbital (LUMO) energy levels of sensitizer dyes are by judiciously, varying the donor fragments and/or the conjugation of the π-spacer. Here, we report the facile synthesis and DSSC performance of a series of organic D–A–π–A type sensitizers based on the PP derivatives, containing triphenylamine/octyloxytriphenylamine as donors and cyanoacrylic acid as acceptors (**PP-I** and **APP-I–IV**, as shown in Fig. 1) are reported for the first time. This work aims to demonstrate how the variation of the donor structure and/or the heterocyclic linkers (thiophene, furan and benzene) impacts the overall photo conversion efficiency of these dyes.

Alkoxyl chains or aryl groups were introduced into the triphenylamine donor or the PP unit to prevent aggregation of the dyes.[8b] The synthetic procedure to obtain the five PP-based dyes involves three major steps as shown in Scheme S1.†

Results and discussion

Synthesis

A two-step Suzuki coupling reaction with a dibromo-PP derivative resulted in the corresponding aldehyde precursors (**4a–e**) and Knoevenagel condensation with cyanoacetic acid, as shown in Scheme S1.† In the Suzuki coupling reaction, preferential oxidative coupling occurs at the more electron deficient 4-carbon position of pyridine derivates leading to the pyridal
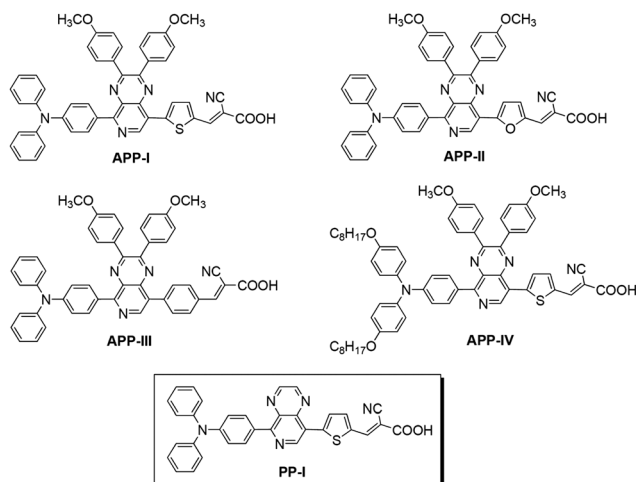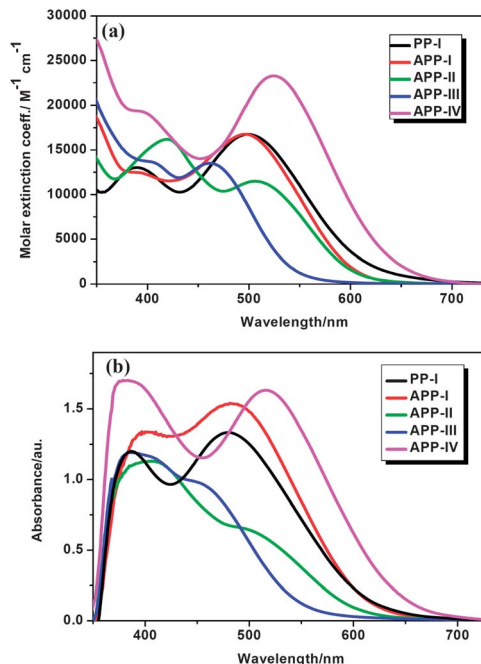
Fig. 2 (a) Absorption spectra of dyes in CH_2Cl_2; (b) absorption spectra of dyes on a 4 μm thin TiO_2 films.

N-atoms proximal to the donor.[19] It is important to highlight the regio-chemistry of **3a–c**, where the pyridal N-atoms of each PP acceptor unit are orientated towards the triphenylamine donor moiety (proximal configuration). This conformation is observed from the corresponding ^{1}H NMR (shown in Fig. S1†), as the δ data of the benzene attached to the PP-core shifted down-field (8.22–8.07 ppm), strongly affected by the nearby pyridal N-atoms. Such a phenomenon has also been observed in other small molecules containing a pyridine ring.[20] All key intermediates and five organic PP-based sensitizers were fully characterized with ^{1}H NMR, ^{13}C NMR, and HRMS (see the ESI†).

Ground-state features

The absorption spectra of PP-based dyes in CH_2Cl_2 and as adsorbed onto 4 μm TiO_2 films are shown in Fig. 2. Their absorptions, molar extinction coefficients, and HOMO–LUMO energy levels are summarized in Table 1. The UV-vis spectra exhibit two major prominent bands, one appearing at 360–400 and the other at 480–530 nm. The former can be ascribed to a localized aromatic π–π* transition from the triarylamine group to the PP moiety. The absorption at 480–530 nm may be attributed to the ICT transition from the triarylamine donor group to the cyanoacetic acceptor unit. The absorption maxima of **PP-I** and **APP-I** to **IV** appear at 500, 497, 506, 461, and 524 nm, respectively. A comparison of the absorption spectra of **PP-I** and **APP-I**, which differ solely by their PP cores, reveals very similar absorption properties, which suggests that changing the PP unit has hardly any effect on the shape of the spectra.

On the contrary, varying the π-bridges (thiophene, furan and benzene) as is done for the three dyes **APP-I** to **III** leads to significant differences in the absorption features demonstrating

Fig. 1 Molecular structures of the synthesized dyes.

Table 1 Optical and electrochemical properties of dyes

Dye	$\lambda_{max}{}^a$/nm ($\varepsilon \times 10^{-4}$ M cm)	$\lambda_{max}{}^b$/nm	HOMO^c/V (vs. NHE)	$E_{0-0}{}^d$/eV	LUMO^e/V (vs. NHE)
PP-I	423 (2.80) 500 (1.67)	479	1.12	2.06	−0.94
APP-I	396 (1.24) 497 (1.68)	482	1.12	2.07	−0.95
APP-II	431 (1.80) 506 (1.15)	499	1.11	2.08	−0.97
APP-III	396 (1.79) 461 (1.35)	446	1.13	2.25	−1.12
APP-IV	429 (2.20) 524 (2.33)	516	0.85	1.95	−1.10

^{a} Absorption maximum in CH_2Cl_2 solution (3×10^{-5} M). ^{b} Absorption maximum on TiO_2 film. ^{c} HOMO potentials measured vs. Fc$^+$/Fc were converted to those vs. the normal hydrogen electrode (NHE) by addition of +0.63 V. ^{d} E_{0-0} was estimated from the intercept of the normalized absorption and emission spectra in each solvent used. ^{e} LUMO is calculated by subtracting E_{0-0} from the HOMO.
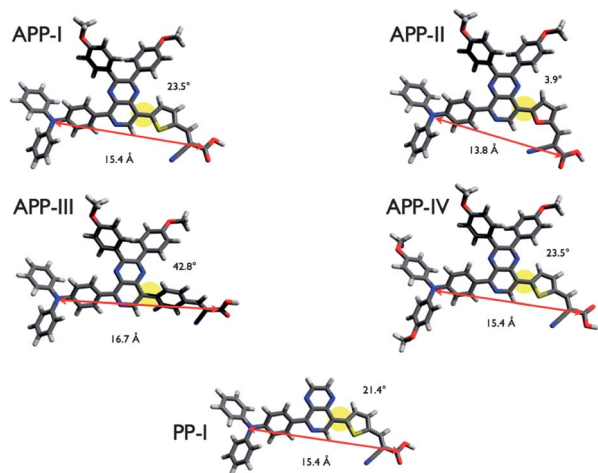
Fig. 3 B3LYP/6-31G* molecular geometries of all PP sensitizers as resulted from DFT calculations. The arrows indicate the varying center-to-center distances from the triarylamine nitrogen atom to the carboxylic acid carbon of the anchoring group. The dihedral angles between the π-spacer and the PP cores are indicated on top of the structures.

that modulation of the electron density of D–A–π–A type dyes may be achieved through alterations of the π-bridges. Strikingly, modifying the triarylamine donor structure results in rather distinct spectral shifts. Upon changing the triphenylamine unit (**APP-I**) to a 4-octoxy-N-(4-octoxyphenyl)-phenylbenzeamine unit (**APP-IV**) the absorption edge shifts to the red by 27 nm. The reason behind this spectral shift is that the two octyloxy groups attached to the triphenylamine electron donor in **APP-IV** enhance the extent of electron delocalization over the entire donor moiety increasing the π-conjugation length, which, in turn, lowers the HOMO–LUMO gap, red-shifting the spectrum. Compared with the solution spectra, the maximum absorption peaks of **PP-I** and **APP-I–IV** on the 4 μm thin transparent TiO_2 films shift to the blue by 21, 15, 13, 15, and 8 nm, respectively (Table 1). The blue shift in the absorption spectra of dyes adsorbed on the surface of the TiO_2 film may be ascribed to the deprotonation of the carboxylic acid.[21]

Cyclic voltammetric data for the **PP-I** and **APP-I** to **IV** dyes is shown in Table 1 and Fig. S2.† The redox potentials (E_{ox}) of **PP-I** and **APP-I** to **IV** corresponding to the HOMO level energy, are located at 1.12, 1.12, 1.11, 1.13, and 0.85 V, respectively, vs. a normal hydrogen electrode (NHE). These values are more positive

than the redox potential of the I^-/I_3^- redox couple (0.4 V vs. NHE) guaranteeing efficient dye regeneration. Interestingly, the HOMO level of **APP-IV** is less positive than those of the other dyes, which is ascribed to the stronger electron donor ability of the octyloxydiphenylamine unit. The zero–zero transition energies (E_{0-0}) of the five dyes were determined to be 2.06, 2.07, 2.08, 2.25, and 1.95 V, respectively, which is estimated from the intercept of normalized absorption and emission spectra. The estimated excited-state potentials corresponding to the LUMO levels, calculated from E_{HOMO} to E_{0-0}, are −0.94, −0.95, −0.97, −1.12, and −1.10 V vs. NHE, respectively. The obtained LUMO values are much more negative than the Fermi level of TiO_2 (−0.5 V vs. NHE), ensuring an efficient electron injection process from the excited state of the dyes into the TiO_2 electrode.

Theoretical approach

Density functional theory (DFT) calculations were carried out to gain further insight into the molecular structures and the electronic distribution of the frontier molecular orbitals of the dyes. The structures of all dyes were optimized using the B3LYP[22] functional with the 6-31G*[23] basis set as implemented in the Gaussian 09[24] suite of programs. All octyloxy groups have been replaced with methoxy groups to save calculation time. The resulting geometries are shown in Fig. 3. Apparently, the variation of the π-linker between the PP moiety and the cyanoacrylic acid anchoring moiety results in a variation of the distance between the triarylamine nitrogen and the carboxylic acid of the anchoring group. The geometry of the furan ring in **APP-II** obliges the molecular structure to bend with respect to the anchoring group, whereas the phenyl ring in **APP-III** results in a stretched configuration of the dye structure. The thiophene spacer in **APP-I**, **APP-IV** and **PP-I** forces the molecules to adopt an intermediate geometry somewhere in-between that of the bent conformation of **APP-II** and the stretched confirmation of **APP-III**. Apart from a change in the distance between the electron donating triarylamine unit and the electron accepting anchoring group, such geometrical variations will have an impact on the adsorption geometries on TiO_2. For instance, closer contacts to the TiO_2 surface as imposed by the structures of **APP-I**, **APP-II**, **APP-IV** and **PP-I** may render back-electron transfer more likely than in the stretched **APP-III** dye. The phenyl ring in **APP-III** induces a significant increase of the dihedral angle between the PP-unit and the π-spacer to a value of 42.8°, which is nearly 20° more
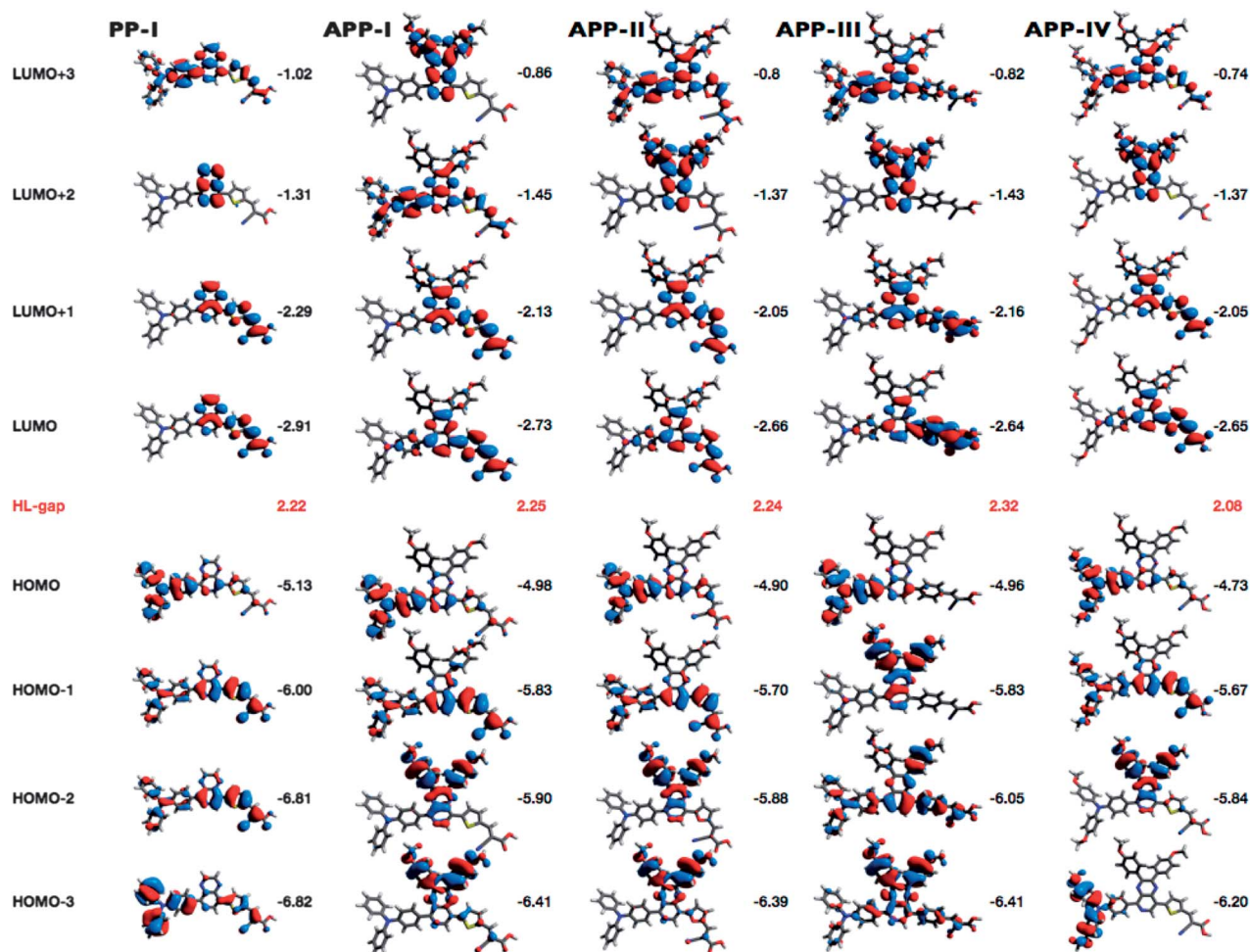
Fig. 4 Representations of the electron densities of the four highest occupied molecular orbitals (HOMO to HOMO−3) and the four lowest unoccupied molecular orbitals (LUMO to LUMO+3) as resulted from B3LYP/6-31G* geometry optimization of all PP sensitizers. The corresponding HOMO−LUMO energy gaps are given in red.

than that found with **APP-I** (23.5°). Consequently, the overlap of the p-orbitals of the spacer and the PP-moiety is reduced in **APP-III** as compared to the other dyes.

The influences of the variations of the chemical structure are further apparent when considering the electronic properties of the dyes, *i.e.* the frontier orbitals and their energies. The four highest occupied molecular orbitals (HOMOs) and lowest unoccupied molecular orbitals (LUMOs) with their corresponding energies and the HOMO–LUMO gaps are depicted in Fig. 4. All dyes exhibit a typical donor–acceptor-type architecture with the HOMO concentrated on the electron donating triarylamine moiety and the LUMO on the electron accepting cyanoacrylic acid anchor.

Detailed considerations on the orbital energies and their electron density distribution (see ESI†) come to the conclusion that the absorption characteristics and excited state features will mainly be dominated by charge transfer transitions from the HOMO to LUMO and to higher LUMO orbitals. This is in conjunction with former results from TD-DFT calculations on similar quinoxaline-based D–A–π–A sensitizers.[7,13b] Furthermore, attaching the octyloxy groups significantly extends the π-conjugation of the donor in **APP-IV**, which raises the HOMO energy

and facilitates its oxidation. As a consequence, **APP-IV** exhibits the lowest HOMO–LUMO energy gap (2.08 eV) among all dyes, which, in turn, corresponds well with the red shift of the absorption spectra (Fig. 2).

Photovoltaic performance

The DSSC performances of all the dyes were tested under AM 1.5G irradiation (1 sun, 100 mW cm^{-2}). To prevent inflated photocurrents arising from stray light, a black metal mask surrounded the active area.[25] The photocurrent density voltage curves (J–V) and the incident photon to current conversion efficiency (IPCE) spectra of the DSSCs based on the PP dyes are shown in Fig. 5. The detailed parameters of short-circuit current density (J_{sc}), open-circuit voltage (V_{oc}), fill factor (ff), and power conversion efficiency (PCE) are collected in Table 2. Hereby, the influence of altering the PP core, π-bridges and donors on the DSSC characteristics is put into focus. When compared with **PP-I**, **APP-I** shows both higher J_{sc} and V_{oc} due to higher electron injection efficiency (87.4 *vs.* 52.6, shown in Table S1†) and less aggregation due to the insertion of the 4-methoxyphenyl groups
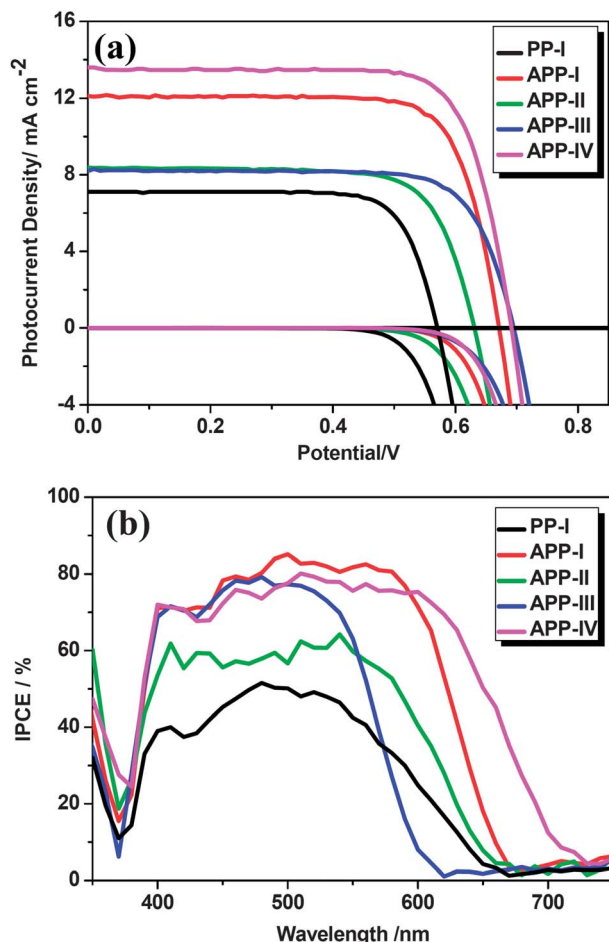
Fig. 5 (a) $J–V$ curves for DSSCs based on the dyes under illumination of AM 1.5G simulated sunlight (100 mW cm^{-2}). (b) IPCE spectra of the same DSSCs.

Table 2 Photovoltaic performance of the dyes[a]

Dye	J_{sc} (mA cm^{-2})	V_{oc} (mV)	ff	η (%)
PP-I	7.10	570	0.76	3.11
APP-I	12.11	671	0.76	6.14
APP-II	8.37	631	0.73	3.93
APP-III	8.20	694	0.76	4.35
APP-IV	13.56	691	0.76	7.12

[a] Electrolyte: 0.03 M I$_2$, 0.05 M LiI, 0.5 M TBP, 0.1 M GNCS, 1.0 M DMII in acetonitrile and valeronitrile (v/v, 85/15).

on the PP unit. This phenomenon can also be understood by the fact that the **APP-I** based cells show a much higher IPCE value than the **PP-I** based cells in the range of 400–600 nm.

Furthermore, the effect of varying the π-bridges is highlighted in terms of the changes in V_{oc}. Scrutinizing the dyes with different linkers (**APP-I** with thiophene, **APP-II** with furan, and **APP-III** with benzene), it is apparent that the V_{oc} of **APP-III** is higher than those of the **APP-I** and **APP-II** based devices. This may be caused by the introduction of a benzene group, which leads to a reduction of electron recombination and improves the V_{oc} due to the relatively large dihedral angle between the PP
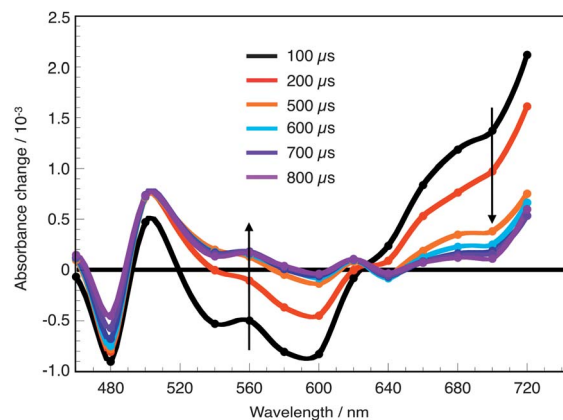
Fig. 6 Transient absorption spectra measured upon nanosecond laser excitation ($\lambda_{exc} = 530$ nm) of **PP-I** adsorbed on 4 μm mesoporous TiO$_2$ films in the absence of redox electrolyte at various delay times between 100 μs and 1 ms. All dyes show comparable spectral signatures.
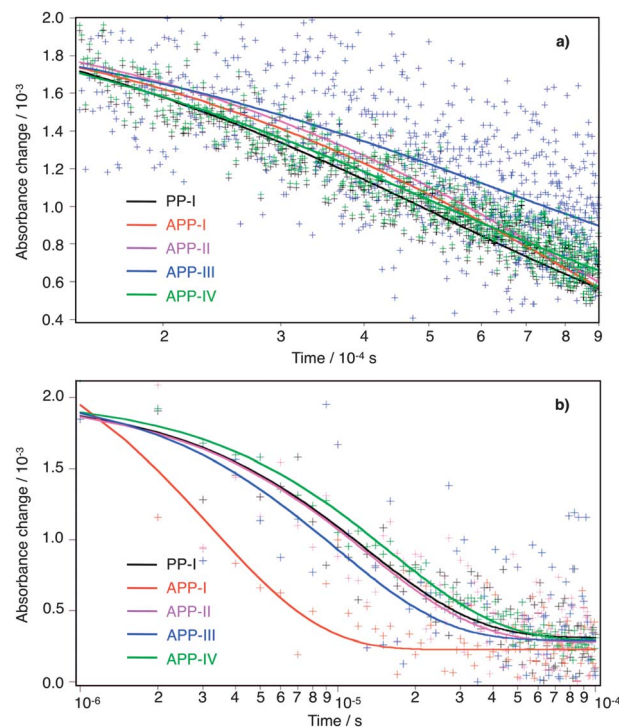
Fig. 7 Transient absorbance decays of the oxidized state after nano-second flash photolysis ($\lambda_{exc} = 530$ nm) of the PP sensitizers adsorbed on 4 μm nanocrystaline TiO$_2$ films. The kinetics was monitored at 680 nm, (a) in the absence (no iodide electrolyte added) and (b) in the presence of the redox electrolyte Z960 under similar conditions.

unit and the benzene-bridge (see Theoretical approach). Such a phenomenon has been also observed in other dyes.[10] It should be noted that the PCE of the **APP-III** based cell was not the highest due to its relatively narrow absorption range and the lower J_{sc}. In general, the J_{sc} is related to the molar extinction coefficients and the absorption spectra of the dyes. Accordingly, a higher molar extinction coefficient yields a higher short-circuit current. The photocurrent of the **APP-IV** cell with

Table 3 Transient absorbance half-reaction decay times of the oxidized states of **PP-I**, **APP-I**, **APP-II**, **APP-III** and **APP-IV** sensitizers in the absence ($t_{1/2,\text{rec}}$) and the presence of the redox electrolyte Z960 ($t_{1/2,\text{reg}}$) as calculated from the temporal analysis of the decay curves at 680 nm

	PP-I	APP-I	APP-II	APP-III	APP-IV
$t_{1/2,\text{rec}}$	405 µs	450 µs	490 µs	600 µs	410 µs
$t_{1/2,\text{reg}}$	9.8 µs	3.1 µs	9.5 µs	7.5 µs	10.6 µs

4-(bis(4-octoxylphenyl)amino)phenyl as electron donor was higher than that for the **APP-I** which contains the triphenylamine as donor. This may be attributed to the higher molar extinction coefficient and the broader absorption of **APP-IV**, which yields better light harvesting and higher J_{sc}. In addition, the much more negative LUMO energy level of **APP-IV** leads to a better electron injection efficiency (82.9 *vs.* 87.4, shown in Table S1†) from the excited state of the sensitizer to the conduction band (CB) of TiO$_2$. Moreover, the **APP-IV** based cells show higher V_{oc} than the **APP-I** cells. This could be explained by the fact that the two octyloxy chains on the 4-(bis(4-octyloxyphenyl)amino)phenyl of **APP-IV** help to form a blocking layer which limits the access of I$_3^-$ ions to the TiO$_2$ electrode surface, hence increasing the electron lifetime and the V_{oc}. The J_{sc} values of all five of the devises are consistent with the resulting IPCEs.

Laser studies

Nanosecond laser flash photolysis measurements were carried out to observe the impact of the structural modifications on the reaction rates of both the charge recombination between the injected electron e_{cb}^- and oxidized radical cation of the sensitizer S$^+$ (eqn (2)) and the regeneration of the dye by the redox electrolyte (eqn (3)).

$$\text{S*}|\text{TiO}_2 \rightarrow \text{S}^+|\text{TiO}_2 + e_{\text{cb}}^- \ (\text{TiO}_2) \tag{1}$$

$$\text{S}^+|\text{TiO}_2 + e_{\text{cb}}^- \ (\text{TiO}_2) \rightarrow \text{S}|\text{TiO}_2 \tag{2}$$

$$\text{S}^+|\text{TiO}_2 + \text{D} \rightarrow \text{S}|\text{TiO}_2 + \text{D}^+ \tag{3}$$

$$e_{\text{cb}}^- \ (\text{TiO}_2) + \text{D}^+ \rightarrow \text{D} \tag{4}$$
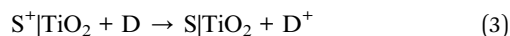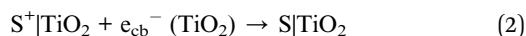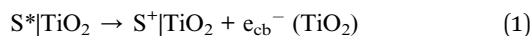
Both reactions follow the ultrafast charge injection from the excited state of the dye S* into the TiO$_2$ conduction band (eqn (1)) and compete kinetically.[26] For these studies, the various sensitizers were adsorbed on 4 µm thick transparent TiO$_2$ films and excited at a wavelength of 530 nm using laser pulses with a duration of 7 ns. In order to scrutinize both processes, *i.e.* the back-electron transfer between the injected electrons and the oxidized state of the dye and the reduction of the latter by the donor D contained in the redox electrolyte (eqn (2) and (3)), the studies were performed in the presence and the absence of the redox electrolyte solution.

All dyes exhibit comparable spectral features in their excited states. A representative transient absorption spectrum of **PP-I** in the absence of the electrolyte is shown in Fig. 6. The broad transient absorption feature developing at wavelengths above 620 nm is characteristic of the triarylamine cation of the oxidized dye molecule S$^+$.[27] Hence, following the decay kinetics of the transient absorption signal measured at 680 nm allowed for the analysis of the charge recombination and dye regeneration rate constants, and for the determination of the half-reaction time of both deactivation processes – $t_{1/2,\text{rec}}$ in the absence of the redox electrolyte and $t_{1/2,\text{reg}}$ in the presence of the redox electrolyte solution.

Upon photoexcitation of the sensitizer, an electron is readily injected into the TiO$_2$ film (eqn (1)). In a pure solvent and in the absence of a donor, the injected electrons have no other possibility than recombining with the oxidized dye cation S$^+$.

Fig. 7a displays the time-profiles of the transient absorption signal measured at 680 nm in the absence of a redox electrolyte for all investigated compounds. The corresponding half-reaction times are listed in Table 3. The results reveal that upon modification of the PP-core, the charge recombination time constants do not change significantly. From current electron transfer dynamics theories, it is expected that the charge recombination rate decreases exponentially when the distance separating the oxide surface from the triarylamine moiety of the dye radical cation is increased, provided the energetics of the process and the associated nuclear reorganization energy are comparable. **APP-III** dye is characterized by a larger distance separating the cyanoacrylate anchor from the amine group (16.7 Å instead of 13.8 Å for **APP-II** and 15.4 Å for **APP-I**, **APP-IV**, and **PP-I**). In this case the time constant for recombination $t_{1/2,\text{rec}}$ is indeed observed to be larger by a factor of ~1.5 compared to the other compounds. This difference, however, is rather small compared to the factor of 5–30 that would be expected for through-space electron transfer with an ET distance elongated by 1.3–2.9 Å and a distance decay constant of 1.2 Å^{-1}. The charge recombination kinetics appears then to be essentially controlled by the conformations of dye molecules adsorbed on the TiO$_2$ surface, which all result in rather similar electron transfer distances.

Considering the dynamics in the presence of the redox electrolyte solution (Fig. 7b), a much faster decay of the dyes' oxidized states was observed, showing that the reduction of dye cations by the redox electrolyte (dye regeneration, eqn (3)) is competing efficiently with the charge recombination process. The dye regeneration of the PP-dye cation occurs within 3–11 µs, indicating that it is *ca.* 2 orders of magnitude faster than charge recombination.

In summary, the laser studies show that the differences observed in the photovoltaic performance of the DSSCs do not depend on the charge recombination in the absence of redox electrolyte or dye regeneration kinetics in the presence of the redox electrolyte. Characteristics such as ground state absorption properties or electronic features of the dyes play a major role in the photovoltaic performance of the dyes. However, charge recombination and dye regeneration are certainly governed by the chemical structures of the dyes – especially with respect to its impact on the adsorption geometry on the TiO$_2$ surface or shielding of the positive charge of the triarylamine cation.

Transient photovoltage and photocurrent as well as electro-chemical impedance (EIS) spectroscopy were performed to

develop a more in-depth understanding about the influence of different dyes on the recombination (eqn (4)), the transport properties and the conduction band edge position of the TiO$_2$ film. The dark current characteristics of the different devices and the parameters such as the transport and the recombination resistance as well as the chemical capacitance, were extracted by fitting the EIS data with the transmission line model, are presented in the ESI (Fig. S3 and S4†). In the low forward bias region, dominated by the FTO–electrolyte interface, the dark current is smallest for **APP-IV** and **APP-II**, followed by **APP-I**, **APP-III** and **PP-I**. At higher forward bias, *i.e.*, around the maximum power point, the smallest dark current is measured for the **APP-III** device and the highest for **PP-I** device, while **APP-I**, **APP-II** and **APP-IV** all show similar mid-range values.

The J_{sc} and V_{oc} values of all the PP devices are tabulated in Table 2. The divergence in the J_{sc} values of various devices can be explained due to the differences in the spectral response of the PP dyes. The device's open-circuit potential (V_{oc}) is influenced by the conduction band (E_{cb}) position and the recombination of electrons at the TiO$_2$–electrolyte interface. The highest value of V_{oc} obtained is for the devices fabricated with **APP-III** and **APP-IV** and the lowest for the **PP-I** device. Plotting the device capacitances against voltage indicates (Fig. 8) that the E_{cb} of the **PP-I** is approximately 45 mV lower than that of the **APP-IV** device. The downward shift of the E_{cb} for the **PP-I** device is partially responsible for the lower V_{oc} (120 mV) measured in comparison with the **APP-IV** device.

The electron lifetime ($\tau_n = C_{chem}R_{ct}$) *versus* the chemical capacitance is plotted for all the devices in order to compare the differences in the electron recombination processes. The chemical capacitance can be used as an indirect measure of the Fermi level, free of IR drop effects (under the assumption of a similar depth of the distribution of the trap states in the DOS) and is, therefore, the preferable representation form for analysing the changes of the electron lifetime.

At higher applied forward bias the electron lifetime is greatest for the **APP-III** device, followed in descending order by **APP-IV**, **APP-I**, **APP-II** and **PP-I** (Fig. 9a) devices. The dyes **PP-I**, **APP-I** and **APP-IV** all contain thiophene as a π-bridge in which **PP-I** is structurally the smallest molecule. **APP-I** has two additional 4-methoxyphenyl groups on the PP unit and **APP-IV** (similar base structure to **APP-I**) contains two additional octyloxy chains on the triarylamine donor moiety. The bulkier the size of the dye, the less of it should adsorb on the TiO$_2$ films. The dye concentration measured on the surface of the TiO$_2$ film for **PP-I** and **APP-I** dyes is similar, but it is lower for the **APP-IV** dye, in agreement with this reasoning. Insertion of 4-methoxyphenyl groups to the structure of **PP-I** to form **APP-I** helped in retarding the electron recombination process. The transformation of the **APP-I** dye structure to **APP-IV** through introduction of octyloxy chains on the donor unit helped further to retard the recombination process. The lowered recombination follows from the reduced access of triiodide present in the redox electrolyte to the TiO$_2$ surface. The electron lifetimes obtained from the transient photovoltage and photocurrent measurements (Fig. 9b) matched well with the electron lifetime trends observed with the EIS measurements.
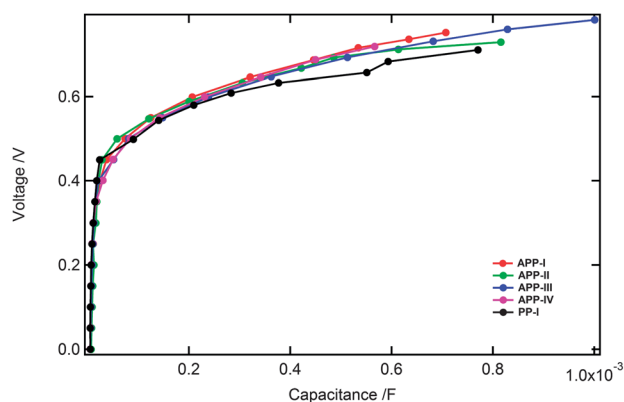
Fig. 8 Applied voltage (corrected for IR drop) plotted *versus* the chemical capacitance determined by impedance spectroscopy.
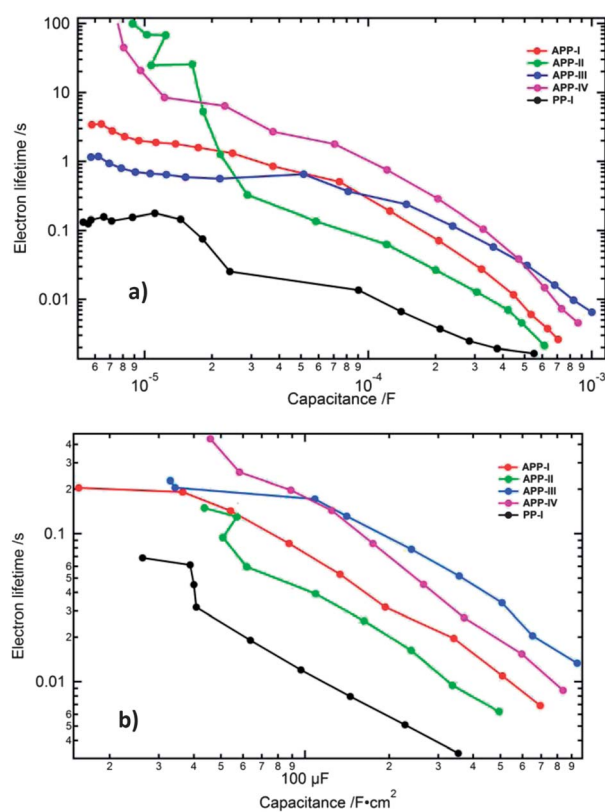
Fig. 9 Electron lifetime plotted *versus* the chemical capacitance (a) from EIS measurements and (b) from the transient photovoltage and photocurrent decay measurements.

Stability measurements

Long-term stability is a vital parameter for sustained cell operation. Substitution of the liquid electrolyte by a solvent-free ionic liquid allows the determination of the stability of the photovoltaic performance over an extended period of time. For the evaluations, **APP-I** and **APP-IV** were utilized as sensitizers in ionic liquid electrolyte DSSCs exploring 1,3-dimethylimidazoliumiodide/1-ethyl-3 methylimidazoliumiodide/1-ethyl-3-methyl-imidazolium tetracyanoborate/iodine/N-butylbenzoimidazole/guanidinium thiocyanate (molar ratio 12/12/16/1.67/3.33/0.67) as redox electrolyte. The

Table 4 Photovoltaic performance parameters of APP-I and APP-IV devices containing solvent-free ionic-liquid electrolyte[a]

Dye	J_{sc} (mA cm^{-2})	V_{oc} (mV)	ff	η (%)
APP-I	9.61	647	0.78	4.96
APP-IV	12.28	648	0.76	6.20

[a] Electrolyte: 1,3-dimethylimidazoliumiodide/1-ethyl-3-methylimidazolium-iodide/1-ethyl-3-methylimidazoliumtetracyanoborate/iodine/N-butyl-benzoimidazole/guanidiniumthiocyanate (molar ratio 12/12/16/1.67/3.33/0.67).

Fig. 10 Stability test illustrating photovoltaic parameter (J_{sc}, V_{oc}, ff, and η) variations with aging time for the devices based on (a) APP-I-, (b) APP-IV-sensitized TiO$_2$ films with a solvent-free ionic-liquid electrolyte during 1 sun visible light irradiation at 60 °C.

devices were subjected to long-term stability tests under the irradiance of AM 1.5G full sun visible light soaking at 60 °C. The detailed photovoltaic parameters of the devices during the aging process are plotted in Fig. 10. The PCE of APP-I and APP-IV dyes containing devices remained at 100% and 97% of the initial value under both the thermal and the light-soaking stress for over 1000 h. This result indicates the underlying potential of PP-based dyes as promising candidates for highly efficient and stable DSSC devices.

Conclusions

In summary, we have synthesized a series of new pyrido[3,4-b]-pyrazine-based metal-free organic dyes and studied the impact of the different substitutions on the PP-core molecule, as well as the utilization of different π-spacers, and various donor moieties on the performance of DSSCs. The photovoltaic experiments show that the methoxyphenyl-substituted PP unit can improve the cells' J_{sc} and V_{oc}, while the use of phenyl π-spacers rather than thiophene or furan moieties results mainly in an increased V_{oc}. Moreover, the introduction of octyloxydiphenyl-amine groups as electron donors resulted in improved J_{sc} and V_{oc}, contributing to the highest PCE (7.12%) for APP-IV based DSSC. EIS and transient photovoltage and photocurrent decay measurements demonstrated that the variations in V_{oc} originated mainly from changes in the recombination behavior. A PCE of 6.20% has been achieved for the APP-IV sensitized DSSC in conjunction with an ionic-liquid electrolyte-based DSSC. This parameter remained at 97% of the initial value following continuous simultaneous thermal and light soaking stress for 1000 h. This work emphasizes the potential of using metal-free organic PP-based dyes for the development of efficient and stable DSSCs. Fine-tuning of the molecular structures provides experimental freedom to attain higher efficiencies and stable DSSC device performance.

Acknowledgements

Notes and references

1 B. O'Regan and M. Grätzel, *Nature*, 1991, **353**, 737–740.
2 (a) M. Grätzel, *Acc. Chem. Res.*, 2009, **42**, 1788–1798; (b) A. Hagfeldt, G. Boschloo, L. C. Sun, L. Kloo and H. Pettersson, *Chem. Rev.*, 2010, **110**, 6595–6663.

photovoltaic parameters of devices using ionic liquid electrolyte measured under standard AM 1.5G full sunlight conditions are summarized in Table 4. These APP-I and APP-IV based DSSCs obtained PCE values of 4.96% and 6.20%, respectively. These

3 (a) F. F. Gao, Y. Wang, D. Shi, J. Zhang, M. K. Wang, X. Y. Jing, R. Humphry-Baker, P. Wang, S. M. Zakeeruddin and M. Grätzel, *J. Am. Chem. Soc.*, 2008, **130**, 10720–10728; (b) Y. M. Cao, Y. Bai, Q. J. Yu, Y. M. Cheng, S. Liu, D. Shi, F. F. Gao and P. Wang, *J. Phys. Chem. C*, 2009, **113**, 6290–6297; (c) C.-Y. Chen, M. K. Wang, J.-Y. Li, N. Pootrakulchote, L. Alibabaei, C. H. Ngoc-le, J. D. Decoppet, J. H. Tsai, C. Grätzel, C. G. Wu, S. M. Zakeeruddin and M. Grätzel, *ACS Nano*, 2009, **3**, 3103–3109; (d) L. Y. Han, A. Islam, H. Chen, C. Malapaka, B. Chiranjeevi, S. F. Zhang, X. D. Yang and M. Yanagida, *Energy Environ. Sci.*, 2012, **5**, 6057–6060; (e) R. Komiya, A. Fukui, N. Murofushi, N. Koide, R. Yamanaka and H. Katayama, Improvement of the conversion efficiency of a monolithic type dye-sensitized solar cell module, *Technical Digest, 21st International Photovoltaic Science and Engineering Conference*, Fukuoka, November 2011, 2 C-50-08.

4 A. Yella, H. W. Lee, H. N. Tsao, C. Yi, A. K. Chandiran, M. K. Nazeeruddin, E. W. G. Diau, C. Y. Yeh, S. M. Zakeeruddin and M. Grätzel, *Science*, 2011, **334**, 629–634.

5 (a) A. Mishra, M. K. R. Fischer and P. Bäuerle, *Angew. Chem., Int. Ed.*, 2009, **48**, 2474–2499; (b) S. Y. Qu, J. L. Hua and H. Tian, *Sci. China: Chem.*, 2012, **55**, 677–697.

6 (a) Y. P. Hong, J.-Y. Liao, D. R. Cao, X. F. Zang, D.-B. Kuang, L. Y. Wang, H. Meier and C.-Y. Su, *J. Org. Chem.*, 2011, **76**, 8015–8021; (b) Y. Hao, X. C. Yang, M. Z. Zhou, J. Y. Cong, X. N. Wang, A. Hagfeldt and L. C. Sun, *ChemSusChem*, 2011, **4**, 1601–1605; (c) Y. Ooyama, Y. Shimada, Y. Inoue, T. Nagano, Y. Fujikawa, K. Komaguchi, I. Imae and Y. Harima, *New J. Chem.*, 2011, **35**, 111–118; (d) S. Haid, M. Marszalek, A. Mishra, M. Wielopolski, J. Teuscher, J.-E. Moser, R. Humphry-Baker, S. M. Zakeeruddin, M. Grätzel and P. Bäuerle, *Adv. Funct. Mater.*, 2012, **22**, 1291–1302.

7 Y. Z. Wu and W. H. Zhu, *Chem. Soc. Rev.*, 2013, **42**, 2039–2058.

8 (a) S. Y. Qu, W. J. Wu, J. L. Hua, C. Kong, Y. T. Long and H. Tian, *J. Phys. Chem. C*, 2010, **114**, 1343–1349; (b) S. Y. Qu, C. J. Qin, A. Islam, Y. Z. Wu, W. H. Zhu, J. L. Hua, H. Tian and L. Y. Han, *Chem. Commun.*, 2012, **48**, 6972–6974.

9 (a) J. X. He, W. J. Wu, J. L. Hua, Y. H. Jiang, S. Y. Qu, J. Li, Y. T. Long and H. Tian, *J. Mater. Chem.*, 2011, **21**, 6054–6062; (b) J. X. He, F. L. Guo, W. J. Wu, X. Li, J. B. Yang and J. L. Hua, *Chem.–Eur. J.*, 2012, **18**, 7903–7915.

10 W. J. Ying, F. L. Guo, J. Li, Q. Zhang, W. J. Wu, H. Tian and J. L. Hua, *ACS Appl. Mater. Interfaces*, 2012, **4**, 4215–4224.

11 (a) W. H. Zhu, Y. Z. Wu, S. T. Wang, W. Q. Li, X. Li, J. Chen, Z. S. Wang and H. Tian, *Adv. Funct. Mater.*, 2011, **21**, 756–763; (b) Y. Z. Wu, X. Zhang, W. Q. Li, Z.-S. Wang, H. Tian and W. H. Zhu, *Adv. Energy Mater.*, 2012, **2**, 149–156.

12 (a) Y. Cui, Y. Z. Wu, X. F. Lu, X. Zhang, G. Zhou, F. B. Miapeh, W. H. Zhu and Z. S. Wang, *Chem. Mater.*, 2011, **23**, 4394–4401; (b) J. Y. Mao, F. L. Guo, W. J. Ying, W. J. Wu, J. Li and J. L. Hua, *Chem.–Asian J.*, 2012, **7**, 982–991.

13 (a) D. W. Chang, H. J. Lee, J. H. Kim, S. Y. Park, S.-M. Park, L. M. Dai and J.-B. Baek, *Org. Lett.*, 2011, **13**, 3880–3883; (b) K. Pei, Y. Z. Wu, Q. Zhang, B. Chen, H. Tian and W. H. Zhu, *Chem.–Eur. J.*, 2012, **18**, 8190–8200.

14 (a) B.-L. Lee and T. Yamamoto, *Macromolecules*, 1999, **32**, 1375–1382; (b) C. J. DuBois and J. R. Reynolds, *Adv. Mater.*, 2002, **14**, 1844–1846; (c) M. Jonforsen, T. Johansson, O. Inganäs and M. R. Andersson, *Macromolecules*, 2002, **35**, 1638–1643; (d) M. Jonforsen, T. Johansson, L. Spjuth, O. Inganäs and M. R. Andersson, *Synth. Met.*, 2002, **131**, 53–59.

15 B. C. Thompson, L. G. Madrigal, M. R. Pinto, T.-S. Kang, K. S. Schanze and J. R. Reynolds, *J. Polym. Sci., Part A: Polym. Chem.*, 2005, **43**, 1417–1431.

16 (a) P.-T. Wu, F. S. Kim, R. D. Champion and S. A. Jenekhe, *Macromolecules*, 2008, **41**, 7021–7028; (b) P.-T. Wu, T. Bull, F. S. Kim, C. K. Luscombe and S. A. Jenekhe, *Macromolecules*, 2009, **42**, 671–681.

17 (a) X. B. Huang, Q. Q. Shi, W.-Q. Chen, C. L. Zhu, W. Y. Zhou, Z. Zhao, X.-M. Duan and X. W. Zhan, *Macromolecules*, 2010, **43**, 9620–9626; (b) Q. Q. Shi, W.-Q. Chen, J. F. Xiang, X.-M. Duan and X. W. Zhan, *Macromolecules*, 2011, **44**, 3759–3765.

18 (a) N. Blouin, A. Michaud, D. Gendron, S. Wakim, E. Blair, R. Neagu-Plesu, M. Belletete, G. Durocher, Y. Tao and M. Leclerc, *J. Am. Chem. Soc.*, 2008, **130**, 732–742; (b) M.-C. Yuan, M.-Y. Chiu, C.-M. Chiang and K.-H. Wei, *Macromolecules*, 2010, **43**, 6270–6277; (c) X. Zhang, J. W. Shim, S. P. Tiwari, Q. Zhang, J. E. Norton, P.-T. Wu, S. Barlow, S. A. Jenekhe, B. Kippelen, J.-L. Bredasa and S. R. Marder, *J. Mater. Chem.*, 2011, **21**, 4971–4982; (d) R. Kroon, R. Gehlhaar, T. T. Steckler, P. Henriksson, C. Muller, J. Bergqvist, A. Hadipour, P. Heremans and M. R. Andersson, *Sol. Energy Mater. Sol. Cells*, 2012, **105**, 280–286.

19 S. T. Handy, T. Wilson and A. Muth, *J. Org. Chem.*, 2007, **72**, 8496–8500.

20 Y. Sun, G. Welch, W. Leong, C. Takacs, G. Bazan and A. Hegger, *Nat. Mater.*, 2012, **11**, 44–48.

21 Z. S. Wang, Y. Cui, Y. Dan-oh, C. Kasada, A. Shinpo and K. Hara, *J. Phys. Chem. C*, 2007, **111**, 7224–7230.

22 P. J. Stephens, F. J. Devlin, C. F. Chablowski and M. Frisch, *J. Phys. Chem.*, 1994, **98**, 11623–11627.

23 V. A. Rassolov, J. A. Pople, M. A. Ratner and T. L. Windus, *J. Chem. Phys.*, 1998, **109**, 1223–1229.

24 M. J. Frisch, *et al.*, Gaussian, Inc., Wallingford CT, 2009.

25 S. Ito, M. K. Nazeeruddin, P. Liska, P. Comte, R. Charvet, P. Pechy, M. Jirousek, A. Kay, S. M. Zakeeruddin and M. Grätzel, *Prog. Photovolt. Res. Appl.*, 2006, **14**, 589–601.

26 M. Sonntag, K. Kreger, D. Hanft, P. Strohriegl, S. Setayesh and D. Leeuw, *Chem. Mater.*, 2005, **17**, 3031–3039.

27 (a) M. Oyama, T. Higuchi and S. Okazaki, *Electrochem. Solid-State Lett.*, 2002, **5**, E1–E3; (b) S. Fantacci, F. De Angelis, M. K. Nazeeruddin and M. Gratzel, *J. Phys. Chem. C*, 2011, **115**, 23126–23133; (c) R. Julio, J. R. Pinzón, D. C. Gasca, S. Gayathri, G. Bottari, T. Torres, D. M. Guldi and L. Echegoyen, *J. Am. Chem. Soc.*, 2009, **131**, 7727–7734.